JOURNAL OF COMPUTATIONAL PHYSICS **134,** 134–149 (1997)
ARTICLE NO. CP975679

Integral Equation Method for the Continuous Spectrum Radial Schrödinger Equation

R. A. Gonzales,*[,1] J. Eisert,†[,2] I. Koltracht,*[,1] M. Neumann,*[,1] and G. Rawitscher†[,3]

*Department of Mathematics, †Department of Physics, University of Connecticut, Storrs, Connecticut 06269-3046
E-mail: rawitsch@uconnvm.uconn.edu

Received December 4, 1996

A new approach to the numerical solution of boundary value problems for differential equations, which originated in recent papers by Greengard and Rokhlin, is improved and adapted to the numerical solution of the radial Schrödinger equation. The approach is based on the conversion of the differential equation into an integral equation together with the application of a spectral type Clenshaw–Curtis quadrature method. Through numerical examples, the integral equation method is shown to be superior to finite difference methods.

I. INTRODUCTION

The Schrödinger equation is one of the most common equations in mathematical physics. Its solution gives the probability amplitude of finding a particle moving in a force field. In the case of a two-body problem, for which, in addition, the force field has spherical symmetry, the corresponding three-dimensional partial differential equation can be reduced to a family of boundary value problems for ordinary differential equations (ODEs),

$$\left[-\frac{d^2}{dr^2}+\frac{l(l+1)}{r^2}+\overline{V}(r)\right]R_l(r)=k^2R_l(r),\qquad 0<r<\infty,\quad l=0,1,2,.... \tag{1.1a}$$

Here k is the wave number, $\overline{V}(r)$ is the given potential, and $R_l(r)$ is the partial radial wave function to be determined, corresponding to the angular momentum number l. In addition, it is required that

$$R_l(0)=0. \tag{1.1b}$$

We shall assume here that $\overline{V}(r)$ is continuous on $(0, \infty)$ and has the following behavior at the endpoints: it tends to zero as fast or faster than $1/r^2$, as $r\to\infty$, and as $r\to 0$ it does not grow faster than $1/r$. Most of the physically meaningful potentials satisfy these conditions. The Coulomb potential is an exception, but it can also be handled by the method described here. Under these conditions on $\overline{V}(r)$, the differential equation (1.1a) is of a limit-point type (Coddington and Levinson [1, p. 256]) and the initial value problem (1.1a) and (1.1b) has a bounded solution on $(0, \infty)$ whose asymptotic behavior depends on normalization. In the physical literature, it is customary to impose the asymptotic condition

$$\lim_{r\to\infty}\left(R_l(r)-\sin\left(kr-\frac{l\pi}{2}\right)-\omega e^{i(kr-l\pi/2)}\right)=0, \tag{1.1c}$$

where ω is an unknown constant uniquely determined by the problem, together with the solution $R_l(r)$. A more detailed description of the Schrödinger equation and its reduction to a family of ODEs can be found, e.g., in Landau [2] and Schiff [3].

For some applications it is preferable to define the S-matrix element, see, e.g. [2, 3], by means of the asymptotic expression

$$\lim_{r\to\infty}(2iR_l-S_le^{i(kr-l\pi/2)}+e^{-i(kr-l\pi/2)})=0,$$

where $S_l=1+2i\omega$.

One of the standard methods used by physicists for the numerical solution of (1.1) is the Numerov method described in Hamming [4]. Although it is simple to use and often produces satisfactory solutions, the method has its drawback common to all explicit finite difference methods, namely roundoff error accumulation puts a lower bound on acceptable step-size. Therefore, if high accuracy is re-

[1] Supported by NSF Grant DMS 9306357.
[2] Supported by J. William Fulbright Foreign Scholarship and in part by a grant from DAD and from a summer grant from the UCONN Research Foundation.
[3] Contact person.

0021-9991/97 $25.00

quired, this method and other finite difference methods can become unsuitable. Illustrative numerical examples for this are given in Section V.

In this paper we describe an alternative method for the solution of the radial Schrödinger equation which gives high accuracy at a cost comparable to that of the Numerov algorithm. The method is based on the reformulation of the boundary value problem (1.1) as an integral equation which is then discretized via the open composite Clenshaw–Curtis quadrature [5]. This integral equation method originated in papers by Greengard [6] and Greengard and Rokhlin [7] and is improved here and adapted to the specific features of the Schrödinger equation. This is a spectral-type numerical method and therefore it displays, typical for spectral methods (Gottlieb and Orszag [8]), superalgebraic convergence when $\overline{V}(r)$ is analytic.

In our treatment we replace the boundary value problem (1.1) by the integral equation

$$\varphi_T(r) + \frac{1}{k}\sin(kr)\int_r^T \cos(kr')V(r')\varphi_T(r')\,dr' + \frac{1}{k}\cos(kr)\int_0^r \sin(kr')V(r')\varphi_T(r')\,dr' = \sin(kr), \quad 0 < r < T, \tag{1.2}$$

where

$$V(r) = \overline{V}(r) + \frac{l(l+1)}{r^2}. \tag{1.3}$$

The solution of (1.2), $\varphi_T(r)$, differs from R_l by a constant multiple which can be recovered without difficulty from the condition (1.1c) for a sufficiently large T as we shall explain in Section II.

A similar Lippmann–Schwinger type integral equation for negative energies has been used in Buendia, Guardiola, and Montoya [9] for computing bound state solutions. In fact, our Eq. (1.2) is a truncated version of the rigorous Lippmann–Schwinger equation and is of a type of integral equations used by Greengard and Rokhlin for boundary value problems on finite intervals.

In Section III we describe in detail the numerical method for solving (1.2) on $[0, T]$. The $(1/r^2)$ singularity at the origin is handled numerically without difficulty. Using power series expansion near the origin, one can see that $R_l(r)$ converges to zero at the rate of r^{l+1}. Thus, even for $l = 0$, $\sin(kr')V(r')\varphi_T(r')$ is bounded since $V(r)$ grows as r^{-2} near the origin. The method can be described briefly as follows. The interval $[0, T]$ is partitioned into m subintervals. On each of the subintervals i, $i = 1, 2, ..., m$, the restricted integral equation is solved twice to give two local solutions $y_i(r)$ and $z_i(r)$. It is shown that the global solution $\varphi_T(r)$ is a linear combination of the local solutions for r restricted to any subinterval i, namely

$$\varphi_T(r) = A_i y_i(r) + B_i z_i(r),$$

where A_i and B_i are constants yet to be determined. These unknown coefficients A_i and B_i can be found as a solution of a sparse (narrow banded) system of linear equations using, say, Gaussian elimination with partial pivoting in $O(m)$ operations. This technique is always applicable if the subintervals in the partition are chosen sufficiently small. Indeed, for sufficiently small subintervals, the norm of the restricted integral operator becomes less than one and hence, a sum of the identity and such an operator is invertible. By contrast, the method of Greengard and Rokhlin requires solvability of restricted integral equations to subintervals of increasing length. The solvability of these equations cannot be assured for all cases.

In Section IV the local solutions y_i and z_i are obtained at Chebyshev points in the ith subinterval using Clenshaw–Curtis quadrature. Despite the fact that the kernel of (1.2) is not differentiable along the diagonal $r = r'$, this quadrature leads to spectral accuracy of the approximation as explained in [7].

A relatively small number of Chebyshev points, n, is needed to achieve high accuracy in each subinterval (of partition) at the cost of $O(n^3)$. The complexity of this step, $O(mn^3)$, dominates the rest of the computation. The global solution $\varphi_T(r)$ is computed at $N = mn$ points and the overall complexity of this method is therefore $O(n^2N)$.

This is a spectral-type numerical technique. This means that for a fixed interval length the error, as a function of n, decreases faster than any power of n, provided that the function being approximated is infinitely differentiable (which is the case here). This compares favorably with fixed order finite difference and finite element methods. A numerical comparison with an adaptive step-size 6th order finite difference method of Raptis and Cash [10], given in Section V, illustrates this advantage. Yet another advantage of the spectral integration method is that it allows efficient and very accurate evaluation of definite integrals of computed solutions of the Schrödinger equation as is demonstrated in example B of Section V. On the other hand, if finite difference methods (with fixed or variable step-size) are used then the solution is obtained at uniformly (or locally uniformly) spaced support points and hence, only a relatively low order Simpson's quadrature can be used to evaluate such integrals.

We remark that the suggested modification of the Greengard–Rokhlin algorithm is also applicable to two-point boundary value problems other than the one derived from the Schrödinger equation and it also admits a straightforward generalization to systems of integral equations corresponding to systems of differential equation. Pre-

liminary investigations also show that our method admits generalization to nonlocal potentials where the product $\overline{V}(r)R_l(r)$ is replaced by an integral

$$\int \overline{V}(r, r')\, R_l(r')\, dr'.$$

This important generalization, for which finite difference methods can become very cumbersome, has application to a wide class of problems, including three-body problems.

In Section V we present several practical examples demonstrating the effectiveness of the integral equation method (IEM). In order to test the integral equation method we compared it with the standard finite difference Numerov method for the solution of various sample problems. In one example we set $V = l(l+1)/r^2$, in which case the solution is known analytically in terms of Riccati–Bessel functions. The IEM showed much better accuracy than the Numerov method. The best accuracy for the Numerov method was attained at a much larger number of points than that for the IEM with an accuracy which in fact is much worse than that of the IEM. Our experiments also demonstrated excellent numerical properties of the IEM, capable of computing accurately very small entries in an array of values in the presence of relatively large values in the same array (see Table I of Section V). These very small values of the wave function may prove to be quite useful in some astrophysical computations where the reaction rates are small. Similar advantages were observed in the case of a potential which is added to the $l(l+1)/r^2$ potential term and which decays rather slowly at large distances like r^{-4}. Here the numerical integration has to proceed out to distances large enough so that the r^{-4} term becomes negligible, a requirement which severely taxes the Numerov method, but which offers no difficulty to the IEM. We also numerically calculated an overlap integral involving the product of two Riccati–Bessel functions and an exponentially decaying weight factor, for which the analytic solution is known. Here, too, our experiments clearly demonstrated that the IEM is the method of choice when high accuracy in the solution of the Schrödinger equation is required.

A Fortran code of our algorithm is available on request.

II. INTEGRAL EQUATION FORMULATION

We wish to solve the radial part of the Schrödinger equation, with $E > 0$,

$$\left[-\frac{\hbar^2}{2m}\frac{d^2}{dr^2} + \frac{\hbar^2 l(l+1)}{2mr^2} + \mathscr{V}(r) \right] R_l(r) = E R_l(r), \quad (2.1)$$

subject to the conditions (1.1b) and (1.1c). Here r is the radial distance of the particle of mass m to the scattering center, E is the energy, l is the angular momentum number, $\mathscr{V}$ is the potential, and $\hbar$ is Planck's constant divided by 2π. With $k = \sqrt{2mE}/\hbar$, we can write (2.1) as

$$\left[\frac{d^2}{dr^2} + k^2 \right] R_l(r) = V(r) R_l(r), \quad (2.2)$$

where $V(r) = l(l+1)/r^2 + \overline{V}(r)$ and $\overline{V}(r) = (2m/\hbar^2)\,\mathscr{V}(r)$. The following proposition shows that the solution of this differential equation also satisfies an integral equation.

PROPOSITION 1. *Let $R_l(r)$ be the unique solution of* (1.1*a*)–(1.1*c*), *and let*

$$\Phi(r) = \sin(kr) R_l(r) + \frac{1}{k}\cos(kr) R_l'(r), \quad 0 < r < \infty. \quad (2.3)$$

For a fixed $0 < T < \infty$,

(i) *if $\Phi(T) \neq 0$, then the integral equation*

$$\begin{aligned} \varphi_T(r) &+ \frac{1}{k}\sin(kr)\int_r^T \cos(kr')V(r')\varphi_T(r')\,dr' \\ &+ \frac{1}{k}\cos(kr)\int_0^r \sin(kr')V(r')\varphi_T(r')\,dr' = \sin(kr), \end{aligned} \quad (2.4a)$$

has a unique solution,

$$\varphi_T(r) = \frac{1}{\Phi(T)} R_l(r).$$

(ii) *If $\Phi(T) = 0$, then* (2.4*a*) *has no solution, while the homogeneous equation*

$$\begin{aligned} \varphi_T(r) &+ \frac{1}{k}\sin(kr)\int_r^T \cos(kr')V(r')\varphi_T(r')\,dr' \\ &+ \frac{1}{k}\cos(kr)\int_0^r \sin(kr')V(r')\varphi_T(r')\,dr' = 0 \end{aligned} \quad (2.4b)$$

has a nontrivial solution. Each such solution is a scalar multiple of $R_l(r)$.

Proof. Let

$$\begin{aligned} \mu(r) = R_l(r) &+ \frac{1}{k}\sin(kr)\int_r^T \cos(kr')V(r')R_l(r')\,dr' \\ &+ \frac{1}{k}\cos(kr)\int_0^r \sin(kr')V(r')R_l(r')\,dr', \quad 0 \le r \le T. \end{aligned}$$

Differentiating we get

$$\mu'(r) = R_l'(r) + \cos(kr)\int_r^T \cos(kr')V(r')R_l(r')\,dr' - \sin(kr)\int_0^r \sin(kr')V(r')R_l(r')R_l(r')\,dr'.$$

Differentiating one more time and using (2.2), we obtain

$$\mu''(r) = -k^2\mu(r).$$

Thus, $\mu(r) = \alpha \sin(kr) + \beta \cos(kr)$. Since $\mu(0) = 0$ it follows that $\mu(r) = \alpha \sin(kr)$. To find α, multiply $\mu(T)$ by $k \sin(kT)$, multiply $\mu'(T)$ by $\cos(kT)$, and add to get

$$\alpha k = k \sin(kT)R_l(T) + \cos(kT)R_l'(T)$$

or $\alpha = \Phi(T)$. Hence, if $\Phi(T) \neq 0$ then $\varphi_T(r) = (1/\Phi(T))$ $R_l(r)$ satisfies (2.4a). If $\psi(r)$ is another solution of (2.4a) then, again differentiating twice, one can see that $\psi(r)$ satisfies (1.1a) and from (2.4a) it follows that $\psi(0) = 0$. Therefore, $\psi(r)$ must be a scalar multiple of $R_l(r)$ and hence of $\varphi_T(r)$. Thus, $\psi(r) = \varphi_T(r)$ and (i) is proved.

If $\Phi(T) = 0$ then the above argument shows that $\mu(r) = 0$ and, hence, $R_l(r)$ satisfies (2.4b). On the other hand, if $\psi(r)$ satisfies (2.4a) or (2.4b) then $\psi(0) = 0$ and $\psi(r)$ satisfies (1.1a). Hence, $\psi(r)$ is a scalar multiple of $R_l(r)$. Therefore, (2.4a) cannot have a solution, while the only solutions of (2.4b) are scalar multiples of $R_l(r)$. The proposition is proved.

We do not anticipate numerical difficulties in the case when T is near T_0 for which $\Phi(T_0) = 0$. In this case, $\varphi_T(r) = (k/\Phi(T))R_l(r)$ becomes large, but the relative errors in the computed $\varphi_T(r)$ will remain the same regardless of how close T is to T_0. This is similar to the inverse iteration for computing eigenvectors, where one solves a nearly singular linear system of equations, for which the solution is an approximate eigenvector (see Golub and Van Loan [12, Section 7.6]). Illustrative examples corresponding to small $\Phi(T)$ are given in Section V.

How small can T be taken so that the asymptotic constant ω in (1.1c) can be determined to a given accuracy depends on the range of the potential $\mathcal{V}(r)$. Since $\mathcal{V}(r)$ decays faster than $1/r^2$, there is no need to go to distances where $1/r^2$ is negligible. Indeed, if $\mathcal{V}(r)$ is negligible, then $R_l(r)$ satisfies the differential equation

$$\left[\frac{d^2}{dr^2} - \frac{l(l+1)}{r^2} + k^2\right] R_l(r) \approx 0 \tag{2.5}$$

and therefore $R_l(r)$ can be represented as a linear combination of the Riccati–Bessel functions (see Abramovitz and Stegun [13]) which are two linearly independent solutions of (2.5),

$$F_l(r) = zj_l(z) = \sqrt{\frac{\pi z}{2}}\, J_{l+1/2}(z) \tag{2.6}$$

and

$$G_l(r) = -zy_l(z) = -\sqrt{\frac{\pi z}{2}}\, Y_{l+1/2}(z), \tag{2.7}$$

where $z = kr$. Since φ_T is a multiple of R_l, φ_T can also be expressed as a linear combination of F_l and G_l, for T sufficiently large and $r \approx T$. Thus let

$$\varphi_T(r) = \alpha F_l(r) + \beta G_l(r) \tag{2.8}$$

and

$$\varphi_T'(r) = \alpha F_l'(r) + \beta G_l'(r). \tag{2.9}$$

The constants α and β can be determined numerically as follows. Substituting $r = T$ into (2.8) and (2.9), multiplying (2.8) by $\alpha G_l'(T)$ and (2.9) by $\alpha G_l(T)$ one finds

$$\alpha[\varphi_T(T)G_l'(T) - \varphi_T'(T)G_l(T)] = \alpha^2[F_l(T)G_l'(T) - F_l'(T)G_l(T)].$$

Hence

$$\alpha = \frac{\varphi_T(T)G_l'(T) - \varphi_T'(T)G_l(T)}{F_l(T)G_l'(T) - F_l'(T)G_l(T)}, \tag{2.10}$$

where the denominator is nonzero, being the Wronskian of two linearly independent solutions of (2.5). Similarly,

$$\beta = \frac{\varphi_T(T)F_l'(T) - \varphi_T'(T)F_l(T)}{F_l'(T)G_l(T) - F_l(T)G_l'(T)}. \tag{2.11}$$

The values of F_l and G_l and their derivatives are readily available from the recursive relations of the type satisfied by Bessel functions. The value of $\varphi_T'(T)$ is found as follows. In our treatment of (1.3), $\varphi_T(r)$ is obtained numerically as a linear combination of Chebyshev polynomials. The latter,

together with their derivatives, satisfy a 3-term recursive relation which is used to compute both $\varphi_T(T)$ and $\varphi_T'(T)$. (We use open Clenshaw–Curtis quadrature so that the endpoint T is not one of the quadrature points). Given α and β, we can now find the normalization constant N for which $N\varphi_T(r)$ satisfies the condition (2.1c). Indeed, asymptotically, the Riccati–Bessel functions $F_l(r)$ and $G_l(r)$ behave like $\sin(kr - l\pi/2)$ and $\cos(kr - l\pi/2)$, respectively. Hence, from

$$N\alpha \sin\left(kr - \frac{l\pi}{2}\right) + N\beta \cos\left(kr - \frac{l\pi}{2}\right) \sim (1 + i\omega) \sin\left(kr - \frac{l\pi}{2}\right) + \omega \cos\left(kr - \frac{l\pi}{2}\right)$$

we obtain equations for N and ω:

$$N\alpha = 1 + i\omega$$

and

$$N\beta = \omega.$$

Thus,

$$N = \frac{1}{\alpha - i\beta} \tag{2.12a}$$

and

$$\omega = \frac{\beta}{\alpha - i\beta}. \tag{2.12b}$$

A conservative estimate for the truncation limit T can be obtained as follows: Using the method of variation of parameters, one can show that $R_l(r)$ satisfies the integral equation

$$R_l(r) + \frac{1}{k} F_l(r) \int_T^r G_l(r')\overline{V}(r')R_l(r')\,dr' + \frac{1}{k} G_l(r) \int_r^\infty F_l(r')\overline{V}(r')R_l(r')\,dr' = uF_l(r) + vG_l(r), \quad T \le r < \infty. \tag{2.13}$$

Equation (2.13) can be verified directly in a way similar to the proof of Proposition 1. Indeed, it is readily seen that the second derivatives of the left- and right-hand sides of (2.13) coincide for any choices of u and v. To find u and v, substitute $r = T$ into (2.13) and, after differentiating (2.13), substitute $r = T$ once again. This gives a 2×2 system of linear equations for u and v which is nonsingular because its determinant is the Wronskian of F_l and G_l. Now let $\|R_l\|_T = \max_{T \le r < \infty} |R_l(r)|$ and suppose that

$$\frac{2}{k} \int_T^\infty |\overline{V}(r')|\,dr' < \varepsilon. \tag{2.14}$$

Since $F_l(r)$ and $G_l(r)$ are of order unity for large r, we have

$$|R_l(r) - (uF_l(r) + vG_l(r))| \le \frac{1}{k} \int_T^r |\overline{V}(r')R_l(r')|\,dr' + \frac{1}{k} \int_r^\infty |\overline{V}(r')R_l(r')|\,dr'.$$

Hence

$$\frac{|R_l(r) - (uF_l(r) + vG_l(r))|}{\|R_l(r)\|_T} \le \frac{2}{k} \int_T^\infty |\overline{V}(r')|\,dr' < \varepsilon.$$

Thus if ε is a desired error bound in the computed solution, then we can take the smallest T such that (2.14) is satisfied. For such T, for $r \ge T$, the asymptotic behavior (2.5) already attains the relative accuracy ε. A numerical example for a slowly decaying potential $\overline{V}(r) = 1/(r + r^4)$ presented in Section V illustrates this property.

We remark that if the potential $\mathscr{V}(r)$ is a combination of a fast decaying potential $\mathscr{V}_f(r)$ and the Coulomb potential, η/r, viz.,

$$\mathscr{V}(r) = \mathscr{V}_f(r) + \eta/r,$$

where η is a constant; then one can truncate at T where $\mathscr{V}_f(r)$ is negligible and use the Coulomb functions instead of the Riccati–Bessel functions in Eqs. (2.5) to (2.7) to determine the asymptotic constant.

III. REPRESENTATION OF φ_T IN TERMS OF LOCAL SOLUTIONS

For the subsequent applications of the composite Clenshaw–Curtis quadrature for the numerical solution of

(2.4a), it is convenient to consider for $i = 1, ..., m$, the family of restricted integral equations,

$$\begin{aligned} y_i(r) &+ \frac{1}{k}\sin(kr)\int_r^{b_i}\cos(kr')V(r')y_i(r')\,dr' \\ &+ \frac{1}{k}\cos(kr)\int_{b_{i-1}}^{r}\sin(kr')V(r')y_i(r')\,dr' \\ &= \sin(kr), \quad b_{i-1} \le r \le b_i, \end{aligned} \tag{3.1a}$$

and

$$\begin{aligned} z_i(r) &+ \frac{1}{k}\sin(kr)\int_r^{b_i}\cos(kr')V(r')z_i(r')\,dr' \\ &+ \frac{1}{k}\cos(kr)\int_{b_{i-1}}^{r}\sin(kr')V(r')z_i(r')\,dr' \\ &= \cos(kr), \quad b_{i-1} \le r \le b_i, \end{aligned} \tag{3.1b}$$

where $b_0 = 0 < b_1 < \cdots < b_{m-1} < b_m = T$ is some partitioning of the interval $[0, T]$. For a sufficiently fine partitioning, these equations have unique solutions y_i and z_i. We now observe that the solution $\varphi_T(r)$ of (2.4a) on $[b_{i-1}, b_i]$ is a linear combination of y_i and z_i. Indeed, it follows from (2.4a) that for $b_{i-1} \le r \le b_i$,

$$\begin{aligned} \varphi_T(r) &+ \frac{1}{k}\sin(kr)\int_r^{b_i}\cos(kr')V(r')\varphi_T(r')\,dr' \\ &+ \frac{1}{k}\cos(kr)\int_{b_{i-1}}^{r}\sin(kr')V(r')\varphi_T(r')\,dr' \\ &= \left(1 - \frac{1}{k}\int_{b_i}^{T}\cos(kr')V(r')\varphi_T(r')\,dr'\right)\sin(kr) \\ &- \frac{1}{k}\cos(kr)\int_0^{b_{i-1}}\sin(kr')V(r')\varphi_T(r')\,dr'. \end{aligned} \tag{3.2}$$

For $i = 1, ..., m$, let

$$A_i = 1 - \frac{1}{k}\int_{b_i}^{T}\cos(kr')V(r')\varphi_T(r')\,dr' \tag{3.3a}$$

and

$$B_i = -\frac{1}{k}\int_0^{b_{i-1}}\sin(kr')V(r')\varphi_T(r')\,dr'. \tag{3.3b}$$

It follows from (3.1a) and (3.1b) that $A_i y_i + B_i z_i$ satisfies (3.2) and hence

$$\varphi_T(r) = A_i y_i(r) + B_i z_i(r), \quad b_{i-1} \le r \le b_i.$$

Assuming that y_i and z_i are known, we show now how to find A_i and B_i. Let us rewrite (3.3a) as

$$A_i = 1 - \frac{1}{k}\sum_{p=i+1}^{m}\int_{b_{p-1}}^{b_p}\cos(kr')V(r')\varphi_T(r')\,dr'.$$

Since on $[b_{p-1}, b_p]$, $\varphi_T = A_p y_p + B_p z_p$, we can also write

$$A_i = 1 - \sum_{p=i+1}^{m}(cy_p)A_p - \sum_{p=i+1}^{m}(cz_p)B_p, \tag{3.4}$$

where, by definition,

$$(cy_p) = \frac{1}{k}\int_{b_{p-1}}^{b_p}\cos(kr')V(r')y_p(r')\,dr' \tag{3.5}$$

and

$$(cz_p) = \frac{1}{k}\int_{b_{p-1}}^{b_p}\cos(kr')V(r')z_p(r')\,dr'. \tag{3.6}$$

Similarly,

$$B_i = -\sum_{p=1}^{i-1}(sy_p)A_p - \sum_{p=1}^{i-1}(sz_p)B_p, \tag{3.7}$$

with

$$(sy_p) = \frac{1}{k}\int_{b_{p-1}}^{b_p}\sin(kr')V(r')y_p(r')\,dr' \tag{3.8}$$

and

$$(sz_p) = \frac{1}{k}\int_{b_{p-1}}^{b_p}\sin(kr')V(r')z_p(r')\,dr'. \tag{3.9}$$

Note that $A_m = 1$ and $B_1 = 0$. Combining (3.4) and (3.7) for $i = 1, ..., m$, we obtain the following system of linear equations for the A_i's and B_i's,

$$\left(\begin{array}{ccccccc:ccccccc}
1 & cy_2 & cy_3 & \dots & cy_m & & & 0 & cz_2 & cz_3 & \dots & cz_m & & \\
 & 1 & cy_3 & \dots & cy_m & & & & 0 & cz_3 & \dots & cz_m & & \\
 & & 1 & \ddots & cy_m & & & & & 0 & \ddots & cz_m & & \\
 & & & \ddots & cy_m & & & & & & \ddots & cz_m & & \\
0 & & & & 1 & & & 0 & & & & 0 & & \\
\dots & \dots & \dots & \dots & \dots & \dots & \dots & \dots & \dots & \dots & \dots & \dots & \dots & \dots \\
0 & & & & & 0 & & 1 & & & & & 0 & \\
sy_1 & \ddots & & & & & & sz_1 & \ddots & & & & & \\
sy_1 & \ddots & 0 & & & & & sz_1 & \ddots & 1 & & & & \\
sy_1 & \dots & sy_{m-2} & 0 & & & & sz_1 & \dots & sz_{m-2} & 1 & & & \\
sy_1 & \dots & sy_{m-2} & sy_{m-1} & 0 & & & sz_1 & \dots & sz_{m-2} & sz_{m-1} & 1 & &
\end{array}\right)
\begin{pmatrix} A_1 \\ A_2 \\ \vdots \\ A_m \\ B_1 \\ B_2 \\ \vdots \\ B_m \end{pmatrix}
=
\begin{pmatrix} 1 \\ 1 \\ \vdots \\ 1 \\ 0 \\ 0 \\ \vdots \\ 0 \end{pmatrix}. \tag{3.10}$$

For notational convenience we omit the parentheses in definitions (3.5), (3.6), (3.8), and (3.9). This system of linear equations has a unique solution because, otherwise (2.4a) would not be uniquely solvable. Using elementary row operations (e.g., subtracting the second row from the first and then the third row from the second, etc.) Eq. (3.10) can be transformed into a sparse system:

$$\left(\begin{array}{ccccccc:ccccccc}
1 & cy_2-1 & & & & & 0 & & 0 & cz_2 & & & 0 & \\
 & 1 & cy_3-1 & & & & & & & 0 & cz_3 & & & \\
 & & 1 & \ddots & & & & & & & 0 & \ddots & & \\
 & & & \ddots & cy_m-1 & & & & & & & \ddots & cz_m & \\
0 & & & & & & 1 & & 0 & & & & 0 & \\
\dots & \dots & \dots & \dots & \dots & \dots & \dots & & \dots & \dots & \dots & \dots & \dots & \dots \\
0 & & & & & & 0 & & 1 & & & & & 0 \\
sy_1 & \ddots & & & & & & & sz_1-1 & \ddots & & & & \\
 & \ddots & 0 & & & & & & & \ddots & 1 & & & \\
 & & sy_{m-2} & 0 & & & & & & & sz_{m-2}-1 & 1 & & \\
0 & & & sy_{m-1} & 0. & & & & 0 & & & sz_{m-1}-1 & 1 &
\end{array}\right)
\begin{pmatrix} A_1 \\ A_2 \\ \vdots \\ A_m \\ B_1 \\ B_2 \\ \vdots \\ B_m \end{pmatrix}
=
\begin{pmatrix} 0 \\ 0 \\ \vdots \\ 0 \\ 1 \\ 0 \\ 0 \\ \vdots \\ 0 \end{pmatrix}.$$

Changing the order of the variables, we can finally transform the coefficient matrix into the block tridiagonal system,

$$\begin{pmatrix} \mathrm{I} & \mathrm{M}_{12} & & & 0 \\ \mathrm{M}_{21} & \mathrm{I} & \mathrm{M}_{23} & & \\ & \mathrm{M}_{32} & \ddots & \ddots & \\ & & \ddots & \mathrm{I} & \mathrm{M}_{m-1,m} \\ 0 & & & \mathrm{M}_{m,m-1} & \mathrm{I} \end{pmatrix} \begin{pmatrix} A_1 \\ B_1 \\ A_2 \\ B_2 \\ \vdots \\ A_m \\ B_m \end{pmatrix} = \begin{pmatrix} 0 \\ 0 \\ \vdots \\ 0 \\ 1 \\ 0 \end{pmatrix}, \tag{3.11}$$

where each block is a 2×2 matrix and with

$$\mathrm{M}_{i-1,i} = \begin{pmatrix} cy_i - 1 & cz_i \\ 0 & 0 \end{pmatrix}, \quad i = 2, ..., m,$$

and

$$\mathrm{M}_{i,i-1} = \begin{pmatrix} 0 & 0 \\ sy_i & sz_i - 1 \end{pmatrix}, \quad i = 2, ..., m.$$

The coefficient matrix in (3.11) is narrow banded and, therefore, the Gaussian elimination with partial pivoting can be used at the expense of $O(m)$ arithmetic operations only (see [12, Section 5.3]) to solve (3.11).

IV. DISCRETIZATION OF LOCAL EQUATIONS

In this section we describe the numerical technique for discretizing the local equations (3.1). It is based on the Clenshaw–Curtis quadrature which is well suited for computing antiderivatives and, hence, for discretizing integrals present in (3.1). Assume $f(r)$ is a function given in the interval $[-1, 1]$ and define

$$F(r) = \int_{-1}^{r} f(r')\, dr', \quad -1 \le r \le 1.$$

Further, assume that $f(r)$ can be expanded in a finite set of Chebyshev polynomials, i.e.,

$$f(r) = \sum_{j=0}^{n} \alpha_j T_j(r), \quad -1 \le r \le 1, \tag{4.1}$$

where

$$T_j(r) = \cos(j \arccos(r)), \quad j = 0, 1, ..., n,$$

are the Chebyshev polynomials. Clenshaw and Curtis [5] showed that if

$$F(r) = \sum_{j=0}^{n+1} \beta_j T_j(r),$$

then

$$[\beta_0, \beta_1, ..., \beta_n]^{\mathrm{T}} = \mathbf{S}_L [\alpha_0, \alpha_1, ..., \alpha_n]^{\mathrm{T}},$$

where

$$\mathbf{S}_L = \begin{pmatrix} 1 & 1 & -1 & 1 & \dots & (-1)^n \\ & 1 & & & & 0 \\ & & 1 & & & \\ & & & 1 & & \\ & & & & \ddots & \\ 0 & & & & & 1 \end{pmatrix} \times \begin{pmatrix} 0 & & & & & 0 \\ 1 & 0 & -\frac{1}{2} & & & \\ & \frac{1}{4} & 0 & -\frac{1}{4} & & \\ & & \frac{1}{6} & \ddots & \ddots & \\ & & & \ddots & 0 & -\frac{1}{2(n-1)} \\ 0 & & & & \frac{1}{2n} & 0 \end{pmatrix}$$

is the so-called left spectral integration matrix. Here $[\nu]^{\mathrm{T}}$ denotes the transpose of the column vector ν. Similarly, if

$$\tilde{F}(r) = \int_{r}^{1} f(r')\, dr' = \sum_{j=0}^{n+1} \tilde{\beta}_j T_j(r),$$

then

$$[\tilde{\beta}_0, \tilde{\beta}_1, ..., \tilde{\beta}_n]^{\mathrm{T}} = \mathbf{S}_R [\alpha_0, \alpha_1, ..., \alpha_n]^{\mathrm{T}},$$

where the right spectral integration matrix is given by

$$\mathbf{S}_R = \begin{pmatrix} 1 & & & \dots & 1 \\ & -1 & & & 0 \\ & & -1 & & \\ & & & \ddots & \\ 0 & & & & -1 \end{pmatrix}$$

$$\times \begin{pmatrix} 0 & & & & & 0 \\ 1 & 0 & -\frac{1}{2} & & & \\ & \frac{1}{4} & 0 & -\frac{1}{4} & & \\ & & \frac{1}{6} & \ddots & \ddots & \\ & & & \ddots & 0 & -\frac{1}{2(n-1)} \\ 0 & & & & \frac{1}{2n} & 0 \end{pmatrix}.$$

Since $T_j(1) = 1$ for all j, we also have that

$$F(1) = \int_{-1}^{1} f(r')\, dr' = \sum_{j=0}^{n+1} \beta_j. \tag{4.2a}$$

Using (4.1) one can find the Chebyshev–Fourier coefficients, α_j, of $f(r)$ as follows. Let τ_k, $k = 0, ..., n$, denote the zeros of T_{n+1}, viz.,

$$\tau_k = \cos \frac{(2k+1)\pi}{2(n+1)},$$

so that

$$T_j(\tau_k) = \cos \frac{(2k+1)j\pi}{2(n+1)}, \quad k, j = 0, ..., n.$$

Substituting $r = \tau_k$, $k = 0, ..., n$, into (4.1), we obtain that

$$\begin{bmatrix} f(\tau_0) \\ \vdots \\ f(\tau_n) \end{bmatrix} = \mathbf{C} \begin{bmatrix} \alpha_0 \\ \vdots \\ \alpha_n \end{bmatrix}, \tag{4.2b}$$

where $\mathbf{C}$ is a *discrete cosine* transform matrix whose elements are specified by

$$\mathbf{C}_{kj} = T_j(\tau_k), \quad k, j = 0, ..., n.$$

The matrix $\mathbf{C}$ has orthogonal columns, that is,

$$\mathbf{C}^{\mathrm{T}}\mathbf{C} = \operatorname{diag}\left(n, \frac{n}{2}, ..., \frac{n}{2}\right).$$

Therefore,

$$\mathbf{C}^{-1} = \operatorname{diag}\left(\frac{1}{n}, \frac{2}{n}, ..., \frac{2}{n}\right) \mathbf{C}^{\mathrm{T}}.$$

Moreover, the matrix $\mathbf{C}$ (as well as $\mathbf{C}^{\mathrm{T}}$ and $\mathbf{C}^{-1}$) can be applied to a vector at the cost of $O(n \log n)$ arithmetic operations. These and other properties of discrete cosine transforms can be found in Van Loan [14]. Thus the vector

$$[\alpha_0, \alpha_1, ..., \alpha_n]^{\mathrm{T}} = \mathbf{C}^{-1}[f(\tau_0), f(\tau_1), ..., f(\tau_n)]^{\mathrm{T}}$$

can be easily found from values of f at τ_0, ..., τ_n. In particular,

$$\begin{bmatrix} F(\tau_0) \\ \vdots \\ F(\tau_n) \end{bmatrix} = \mathbf{C}\, \mathbf{S}_L \mathbf{C}^{-1} \begin{bmatrix} f(\tau_0) \\ \vdots \\ f(\tau_n) \end{bmatrix} \tag{4.3a}$$

and, similarly,

$$\begin{bmatrix} \tilde{F}(\tau_0) \\ \vdots \\ \tilde{F}(\tau_n) \end{bmatrix} = \mathbf{C}\, \mathbf{S}_R \mathbf{C}^{-1} \begin{bmatrix} f(\tau_0) \\ \vdots \\ f(\tau_n) \end{bmatrix}. \tag{4.3b}$$

We remark that in writing the equality sign in (4.3a) and (4.3b), we assume that β_{n+1} is set to zero. This is an acceptable assumption because $f(r)$ is itself only approximately represented by the polynomial in (4.1) and the overall accuracy of approximation is not affected.

The formulas (4.3) can be generalized for intervals $[b_{i-1}, b_i]$ other than $[-1, 1]$ by the linear change of variable

$$h(t) = \tfrac{1}{2}(b_i - b_{i-1})t + \tfrac{1}{2}(b_i + b_{i-1}).$$

Thus if

$$\tau_j^{(i)} = h(\tau_j), \quad j = 0, ..., n,$$

then

$$\begin{bmatrix} F(\tau_0^{(i)}) \\ \vdots \\ F(\tau_n^{(i)}) \end{bmatrix} = \frac{(b_i - b_{i-1})}{2}\, \mathbf{C}\, \mathbf{S}_L \mathbf{C}^{-1} \begin{bmatrix} f(\tau_0^{(i)}) \\ \vdots \\ f(\tau_n^{(i)}) \end{bmatrix} \tag{4.4a}$$

and, similarly,

$$\begin{bmatrix} \tilde{F}(\tau_0^{(i)}) \\ \vdots \\ \tilde{F}(\tau_n^{(i)}) \end{bmatrix} = \frac{(b_i - b_{i-1})}{2}\, \mathbf{C}\, \mathbf{S}_R \mathbf{C}^{-1} \begin{bmatrix} f(\tau_0^{(i)}) \\ \vdots \\ f(\tau_n^{(i)}) \end{bmatrix}. \tag{4.4b}$$

Using (4.4) we can now discretize the local equation (3.1a) as

$$\left[\mathbf{I}+\frac{(b_i-b_{i-1})}{2k}(\mathbf{D}_{s_i}\mathbf{C}\mathbf{S}_R\mathbf{C}^{-1}\mathbf{D}_{c_iv_i}+\mathbf{D}_{c_i}\mathbf{C}\mathbf{S}_L\mathbf{C}^{-1}\mathbf{D}_{s_iv_i})\right]\mathbf{Y}_i=\mathbf{s}_i, \tag{4.5a}$$

where

$$\mathbf{Y}_i=[y_i(\tau_0^{(i)}),\ldots,y_i(\tau_n^{(i)})]^{\mathrm{T}},$$
$$\mathbf{s}_i=[\sin(k\tau_0^{(i)}),\ldots,\sin(k\tau_n^{(i)})]^{\mathrm{T}},$$
$$\mathbf{D}_{c_i}=\mathrm{diag}(\cos(k\tau_0^{(i)}),\ldots,\cos(k\tau_n^{(i)})),$$
$$\mathbf{D}_{s_iv_i}=\mathrm{diag}(\sin(k\tau_0^{(i)})V(\tau_0^{(i)}),\ldots,\sin(k\tau_n^{(i)})V(\tau_n^{(i)})),$$

and, similarly, $\mathbf{D}_{s_i}$ and $\mathbf{D}_{c_iv_i}$. In much the same way

$$\left[\mathbf{I}+\frac{(b_i-b_{i-1})}{2k}(\mathbf{D}_{s_i}\mathbf{C}\mathbf{S}_R\mathbf{C}^{-1}\mathbf{D}_{c_iv_i}+\mathbf{D}_{c_i}\mathbf{C}\mathbf{S}_L\mathbf{C}^{-1}\mathbf{D}_{s_iv_i})\right]\mathbf{Z}_i=\mathbf{c}_i. \tag{4.5b}$$

The solution of (4.5a) and (4.5b) can be done using standard software, e.g., Gaussian elimination with partial pivoting at the cost of $O(n^3)$ arithmetic operations. The solutions Y_i and Z_i give approximate values to the local functions $y_i(r)$ and $z_i(r)$ at the Chebyshev nodes in each of the subintervals $[b_{i-1}, b_i]$, $i=1,\ldots,m$. The inner products (3.5), (3.6), (3.8), and (3.9) can now be obtained using (4.2) as follows:

$$(cy_i)=\frac{b_i-b_{i-1}}{2k}[1,1,\ldots,1]\mathbf{S}_R\mathbf{C}^{-1}\mathbf{D}_{c_iv_i}\mathbf{Y}_i,$$
$$(cz_i)=\frac{b_i-b_{i-1}}{2k}[1,1,\ldots,1]\mathbf{S}_R\mathbf{C}^{-1}\mathbf{D}_{c_iv_i}\mathbf{Z}_i,$$
$$(sy_i)=\frac{b_i-b_{i-1}}{2k}[1,1,\ldots,1]\mathbf{S}_L\mathbf{C}^{-1}\mathbf{D}_{s_iv_i}\mathbf{Y}_i,$$
$$(sz_i)=\frac{b_i-b_{i-1}}{2k}[1,1,\ldots,1]\mathbf{S}_L\mathbf{C}^{-1}\mathbf{D}_{s_iv_i}\mathbf{Z}_i.$$

The computation of each of these inner products takes $O(n)$ arithmetic operations after $[1,1,\ldots,1]\mathbf{S}_{L,R}\mathbf{C}^{-1}$ is precomputed at the cost of $O(n^3)$ flops and is negligible, relative to the cost of solving (4.5). These inner products are substituted into (3.11) and the weights A_i, B_i are obtained at the cost of $O(m)$ arithmetic operations. The coefficient in $O(m)$ is of order unity and hence much smaller than n^3 in $O(n^3m)$ needed to compute $\mathbf{Y}_i$, $\mathbf{Z}_i$, $i=1,\ldots,m$. Thus the overall cost of the computation is dominated by the $O(n^3m)$ cost of solving local equations (4.5). The cost of solving local equations can be reduced by the use of parallel processors since the calculation of $\mathbf{Y}$ and $\mathbf{Z}$ on each subinterval is independent.

Using the sparseness of $\mathbf{S}_L$ and $\mathbf{S}_R$ and the fast implementation of the discrete cosine transform, one may also try to reduce the cost of solving (4.5) by the use of iterative algorithms. This will be investigated separately.

After A_i and B_i are found we finally obtain

$$\begin{bmatrix}\varphi_T(\tau_0^{(i)})\\ \vdots\\ \varphi_T(\tau_n^{(i)})\end{bmatrix}\approx A_i\mathbf{Y}_i+B_i\mathbf{Z}_i.$$

To estimate the accuracy of approximation, we use the following property of Chebyshev expansions.

PROPOSITION 2. *Let $f\in C^p[-1,1]$, $p>1$ and*

$$f(r)=\sum_{j=0}^{\infty}\alpha_jT_j(r),\quad -1\le r\le 1.$$

Then

$$|\alpha_j|\le\left\{\frac{2}{\pi}\int_0^{\pi}\left|\frac{d^p}{d\theta^p}f(\cos\theta)\right|d\theta\right\}\frac{1}{j^p}=\frac{c}{j^p}$$

and

$$\left|f(r)-\sum_{j=0}^{n}\alpha_jT_j(r)\right|\le\frac{c}{p-1}\frac{1}{n^{p-1}}.$$

The proof of this proposition is outlined in [8, p. 29]. It implies that if $f(r)$ is analytic then the convergence of the Chebyshev expansion is superalgebraic.

Using this proposition, one can show (see [7]) the following.

THEOREM 1. *Suppose $V(r)$ is $(p+1)$-times continuously differentiable for $0<r<\infty$. Let φ_T be the solution of (2.4a) and let A_i, B_i, $\mathbf{Y}_i$, and $\mathbf{Z}_i$ be the solutions of (3.10), (4.5a), and (4.5b), respectively. Then*

$$\left\|\begin{bmatrix}\varphi_T(\tau_0^{(i)})\\ \vdots\\ \varphi_T(\tau_n^{(i)})\end{bmatrix}-(A_i\mathbf{Y}_i+B_i\mathbf{Z}_i)\right\|_{\infty}\le\frac{\mathscr{C}_p}{n^p},$$

where $\tau_0^{(i)},\ldots,\tau_n^{(i)}$ are the Chebyshev points in the corresponding subintervals of partition and $\mathscr{C}_p$ is a constant which depends on p only.

This spectral-type high accuracy of approximation of φ_T with $A_i\mathbf{Y}_i + B_i\mathbf{Z}_i$, for modest values of n, is illustrated with numerical examples in the next section. The high accuracy of approximation here is due to the special feature of Clenshaw–Curtis quadrature, the highly accurate computation of the antiderivative. Since the kernel of the integral equation (3.1) is not smooth across the diagonal $\{r = r'\}$, the standard Nystrom-type discretization methods will fail to give high accuracy in this case (see, e.g., Delves and Mohamed [15]).

Some Gauss-type quadratures can be used instead of the Clenshaw–Curtis quadrature with similar results, most notably the Gauss–Legendre quadrature for which a proposition similar to Proposition 2 is valid (Gottlieb and Orszag [8, p. 37]). We prefer the former because the support points are readily available algebraically, rather than from tables as Legendre points, the transition from values of a function to its expansion coefficients and vice versa in (4.2b) can be done with the fast cosine transform and the transition matrices from expansion coefficients of a function to its antiderivatives, $\mathbf{S}_L$, $\mathbf{S}_R$ are so simple due to trigonometric identities enjoyed by Chebyshev polynomials (see Clenshaw and Curtis [5]).

Finally, we remark that the values of φ_T are found inside each of the subintervals of partition at Chebyshev nodes $\tau_0^{(i)}, \ldots, \tau_n^{(i)}$. The value of φ_T at T (or any other point in $[0, T]$, for that matter) can be found as follows. Using $\mathbf{C}^{-1}$ we can find Chebyshev–Fourier coefficients in $[b_{i-1}, b_i]$,

$$\begin{bmatrix} \alpha_0^{(i)} \\ \vdots \\ \alpha_n^{(i)} \end{bmatrix} = \mathbf{C}^{-1} \begin{bmatrix} \varphi_T(\tau_0^{(i)}) \\ \vdots \\ \varphi_T(\tau_n^{(i)}) \end{bmatrix}.$$

Thus,

$$\varphi_T(r) = \sum_{j=0}^{n} \alpha_j^{(i)} T_j(h_i(r)), \quad b_{i-1} \le r \le b_i.$$

The value of $\varphi_T(r)$ (or $\varphi_T'(r)$) for $r \neq \tau_k^{(i)}$ can be found using the recursion satisfied by Chebyshev polynomials,

$$T_{j+1}(x) = 2xT_j(x) - T_{j-1}(x).$$

In fact, we have used a backward (numerically more reliable) recursion suggested in [5].

V. NUMERICAL EXAMPLES

In this section we document the numerical properties of the integral equation method (IEM) by means of several examples. In the first application we choose a case for which the analytic solution is related to a known Riccati–Bessel function and we obtain the accuracy of our method by comparing the numerical answer with the analytic one. Subsequently, we obtain an overlap integral between two such solutions and a weight function for which the answer is again known analytically, in order to test the feasibility of calculating quantum mechanical matrix elements. Both applications bring out the power of the IEM in that the solution has high accuracy and, at the same time, the values of the solution are automatically provided at the Chebyshev points where they are needed for performing the overlap integral according to the Clenshaw–Curtis quadrature procedure. The IEM can also calculate the solution at other points without further loss of accuracy at the cost of $O(n)$ operations per point, where n is the number of Chebyshev points per subinterval (e.g., $n = 16$ in our experiments). In the third case, we apply our method to the calculation of solutions of the Schrödinger equation, for long-range potentials. Finally, we consider the choice of T such that $\Phi(T) \approx 0$. In our examples such choice of T has no effect on the accuracy of the computed solution. All calculations have been done in double precision Fortran on IBM-3090 mainframe. Values of Bessel functions used in our experiments were obtained by calling the International Mathematical Scientific Library (IMSL) subroutines DBSJS and DBSYS.

A. *Solution of the IEM for a Riccati–Bessel Function Case*

We take for the potential V in our integral equation (1.2), the expression

$$V(r) = l(l+1)/r^2 \tag{5.1}$$

in which case the solution is given by the Riccati–Bessel function,

$$F_l(k, r) = zj_l(z), \quad z = kr. \tag{5.2}$$

Here k is the wave number, r is the radial distance, l is the angular momentum number, and $j_l(z)$ is a spherical Bessel function as defined in [13]. We denote the numerical solution of the integral equation (1.2) by $\varphi_T(r)$. In order to obtain a measure of the accuracy of φ_T, we obtain, for comparison, the values of the function F_l from the IMSL, by calling the subroutine DBSJS for the cylindrical Bessel function. The normalization constant N_l is obtained from (2.12a) which requires a call to the IMSL subroutines at $r = T$. The maximum of the absolute value of the difference between the two functions φ_T and F_l, in the range of integration $[0, T]$ is denoted as "Error," and is calculated for the two cases $l = 6$, $k = 1\ fm^{-1}$ and $l = 8$, $k = 40\ fm^{-1}$. In both cases we choose the upper value of the radial range, T, equal to 50 *fm* but it can be chosen arbitrarily

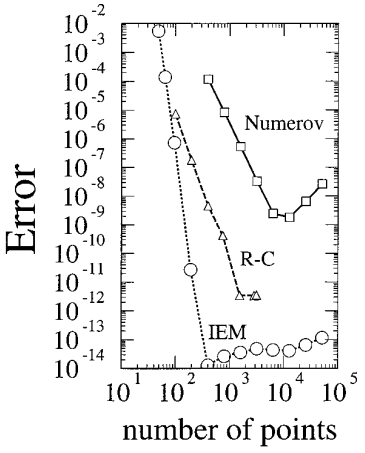

FIG. 1. Error in the numerical calculation of a Riccati–Bessel function, in terms of the number of points in the interval $0 \le r \le 50$ *fm*. The integral equation method, IEM, is represented by circles. The two finite difference methods, the fixed step size method of Numerov and the variable step-size method of Raptis and Cash are represented by squares and triangles, respectively. The Riccati–Bessel function is defined in (5.2), the value of the angular momentum number is $l = 6$, the wave number is $k = 1$ fm^{-1} and the error is obtained by comparison with a Bessel function called through the IMSL library. The calculation is done in Fortran in double precision (approximately 14 significant figures) on an IBM mainframe 3090 computer.

according to the analysis in Section II. The solution of the integral equation is obtained by dividing the integration range $[0, T]$ into m partitions of equal length. The number of Chebyshev points n in each partition is taken at the fixed value of 16, as suggested in [7]. For each successive calculation the number of intervals is increased by a factor of two. The results for the error, for the case $l = 6$, $k = 1\ fm^{-1}$, are shown by the open circles in Fig. 1 as a function of the total number of integration points $16 \times m$. The figure shows that the accuracy begins to improve rapidly once the number of intervals is larger than 3 and the error reaches a minimum value of the order of magnitude of machine accuracy for 25 intervals (400 points). Beyond this point, the accumulation of rounding errors prevent further improvement. As expressed in terms of number of points per oscillation of the function F (i.e., per wavelength, $2\pi/k$) the maximum accuracy is reached for 50 points per oscillation (i.e., $[2\pi/k]/[50/400] \cong 50$).

In order to compare the IEM's accuracy with commonly used finite difference methods, we have also calculated the solution of the corresponding differential equation

$$\left(\frac{d^2}{dr^2} - \frac{l(l+1)}{r^2} + k^2\right) R_l(r) = 0 \qquad (5.3)$$

by the so-called Numerov finite difference method. Since (1.1) is actually an eigenfunction problem, one can start with an arbitrary slope, say $R_l'(0) = 1$, and then to scale the computed solution of the initial value problem to satisfy (1.1c) much in the same way as described in Section II above. In this procedure the radial interval is divided into equally spaced mesh of points with a mesh size h and, by using Taylor expansions for the function and its derivatives, one obtains the approximate value of R_l from the values at two previous points according to the recursion

$$u_n = 2u_{n-1} - u_{n-2} + \frac{h^2}{12}(u_n'' + 10u_{n-1}'' + u_{n-2}''). \qquad (5.4)$$

Here u is the numerical solution of (5.3) and the second derivatives u_i'' are calculated in terms of u_i from (5.3).

The accuracy of Numerov's method, which is of $O(h^4)$ (see Stoer and Bulirsch [16, p. 540]), is shown by means of the open squares in Fig. 1. It is clear from the figure that the accuracy in Numerov's method increases much less quickly with the number of points than the IEM. The maximum accuracy in Numerov's method of 0.2×10^{-8} is reached for 12,800 points and corresponds to a step size of $h = 0.0039$ *fm*. This number of points is 32 times larger than the number required by the IEM to reach its maximum accuracy of $0.13 \times 10^{-13.}$ Moreover, the accuracy itself is worse by five orders of magnitude.

We also compared the IEM with the more sophisticated variable step-size method of Raptis and Cash [10], based on fourth-order Numerov and sixth-order of their own. Similar variable step-size finite difference schemes appeared in recent papers by Simos and Avdelas and Simos; (see [11] and references therein). As expected, being a higher order variable step-size method, it achieves higher accuracy at fewer mesh points than Numerov but still is not able to achieve the accuracy of the IEM. After a certain value of the input tolerance is reached, the further decrease in tolerance does not result in any change in step-size selection and, hence, does not improve the accuracy; see Figs. 1 and 2. The same behaviour has been observed in our numerical experiments (not reported here) with the "summed" Numerov method, recently discussed by Friar [17].

The second case, $l = 8$, $k = 40\ fm^{-1}$, and $T = 50$ *fm* is illustrated in Fig. 2. This case is more probing because the wave number is now 40 times larger. Again, the IEM error decreases rapidly once the number of points is larger or equal to 1600 (100 intervals) and reaches a minimum value of 0.2×10^{-12} for 12,800 points. The average number of points per wavelength of the function is in this case 40. This is slightly smaller than what it was in the previous case, but the accumulation of roundoff errors prevents the maximum accuracy from reaching as high a value as in the first case. Nevertheless, as the number of points increases, the further accumulation of roundoff errors is very small, similar to what was the case in Fig. 1, and illustrates the

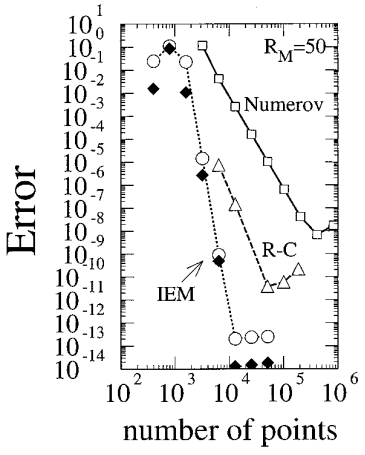

FIG. 2. Same as Fig. 1 for $l = 8$ and $k = 40\ fm^{-1}$. The solid diamonds represent the error of the functions y_i and z_i, defined in Eqs. (3.1) and calculated in each subinterval i. The error is the maximum of the last three Chebyshev coefficients for both y_i and z_i in all intervals.

stability of the IEM. By comparison, Numerov's method requires 409,600 points to reach a maximum accuracy of 0.7×10^{-8}. This number of points is 256 times larger than the number of points where IEM reaches its maximum accuracy.

When an analytic result is not available for comparison with the IEM result, then, as recommended in [5], one can use as a measure of the accuracy of the IEM the magnitude of the last three Chebyshev expansion coefficients of the solution φ_T in each partition which is automatically obtained during the IEM calculation. If the last three coefficients are sufficiently small then the remaining coefficients may be considered negligible (see Proposition 2). This is borne out by our calculations. The maximum for all partitions of the absolute value of the last Chebyshev coefficient in each partition is displayed by means of the solid squares in Fig. 2. One sees that this measure tracks well the actual accuracy achieved by the IEM. A similar pattern of behavior was observed in all the other numerical experiments with IEM (most were not reported here). Therefore we recommend that the optimal choice for the number of subintervals be obtained by finding the minimum on the line of solid points. Further increase in the number of subintervals is not expected to improve the accuracy, but rather it causes an increased accumulation of rounding errors.

The dependence of the accumulation of the roundoff errors on the length of the integration interval, T, is illustrated in Fig. 3. While in Numerov's method the error increases by several orders of magnitude as T is increased from 10 to 50 *fm*, in the IEM the error changes by less than an order of magnitude. This result again supports the insensitivity of the IEM to roundoff errors.

Figures 1 through 3 illustrate the absolute value of the error, but they do not give a good account of the relative error which occurs to the left of the turning point, where the function φ_T becomes very small, of the order of $O(r^{l+1})$. In order to test the error to the left of the turning point, a calculation of the functions $F_l(r)$ was performed with the IEM for $l = 100$, $k = 1$. The value T of the upper cutoff T was taken at 105 *fm* and the number of partitions was taken to be $m = 150$ (the corresponding number of points is 2400, which is 150 points per wavelength or three times the number of points previously needed to reach maximum accuracy in Fig. 1). The normalization of the solution of the IEM was obtained by comparison with the value of F_l, calculated by the series solution in powers of kr at $r = 100$ *fm*, described in 10.1.2 of [13]. The result is compared with values given in [13] and also with values obtained through the IMSL subroutine and listed in Table I. With the exception of the smallest value of r (10 *fm*), the agreement is good to within 11 significant figures with the values listed in [13]. At $r = 10$ *fm*, the IMSL routine returned zeros for the answer, due to underflows.

Table I demonstrates that the IEM method is capable of obtaining accurate small values in the presence of large values. It also demonstrates that the $O(1/r^2)$ singularity of the potential near the origin does not affect the accuracy of the computed solution near the origin noticeably. During the course of this experiment, it also became clear that the Bessel function subroutine present in the IMSL library of the IBM mainframe has a limited range of parameter space. For example, when $x = kr = 10$, the maximum value of l for which IMSL provides answers for the regular Bessel function is 92. For $x = 20$, $l_{\max} = 109$; for $x = 40$, $l_{\max} = 107$; for $x = 60$, $l_{\max} = 47$; for $x = 50$, $l_{\max} = 45$. The IEM,

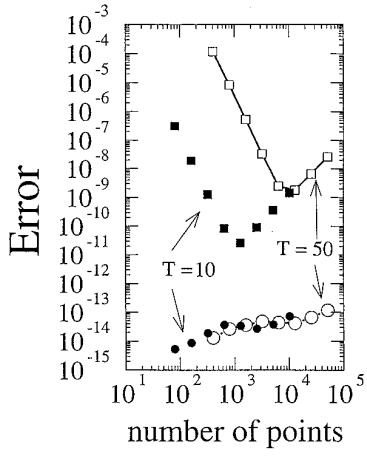

FIG. 3. Dependence of the error on the length of the integration interval T. The squares represent the Numerov's results, the circles represent IEM's results. The solid (open) symbols correspond to $T = 10$ *fm* (25 *fm*). The other parameters are the same as in Fig. 1.

TABLE I

Accuracy IEM for the Riccati–Bessel Function F_l to the Left of the Turning Point

$r(fm)$	F_l^a	Method[b]
10	5.832040182E-90	AS
10	—	IMSL
10	5.832040178E-90	IEM
50	1.019012263E-22	AS
50	1.019012262932E-22	IMSL
50	1.019012262931E-22	IEM
100	1.088047701E-02	AS
100	1.088047701144E-02	IMSL
100	1.088047701143E-02	IEM

[a] The function F_l is defined in (5.2), $k = 1\ fm^{-1}$, $l = 100$.

[b] The entries AS were taken from a Table by [13], the IMSL results are obtained from IMSL subroutine DBSJS, the IEM values are obtained from the IEM code, and are normalized as explained in the text.

however, continued to give accurate values, as compared with [13], beyond this range of IMSL parameter space.

B. *An Overlap Integral*

Here we present a practical example for which high accuracy in the computed solution is essential. Again, to be able to estimate errors exactly we chose, as in Subsection A, $V(r) = l(l+1)/r^2$ so that the solution is known and given by (5.2). The quantities of interest are

$$I_l(k_1, k_2, \lambda) = \int_0^\infty F_l(k_1, r)\,\frac{\exp(-\lambda r)}{r}\,F_{l+2}(k_2, r)\,dr. \quad (5.5)$$

These quantities, for varying values of k_1 and k_2, are inputs in the calculation in momentum space of the scattering T-matrix between two nucleons or a nucleon and a pion. When the energy is high, the range of the wave numbers k_1 and k_2 becomes very large, and severe cancellations occur in the integral. For example, in the case of scattering of two nucleons at energies of the order of tens of GeV, the wave numbers can be as high as $40\ fm^{-1}$ and the angular momentum numbers can be equally high.

In our numerical example we choose $l_1 = 6$, $k_1 = 1\ fm^{-1}$; $l_2 = 8$, $k_2 = 40\ fm^{-1}$, and $\lambda = 0.7\ fm^{-1}$. In this case the maximum of the integrand is $1.45 \times 10^{-3}\ fm^{-1}$, while the resulting integral is 0.27×10^{-10}, a cancellation of seven significant figures.

For comparison purposes this integral can be calculated analytically by means of the recursion relation (see [18])

$$I_{l+1} = \left(\frac{2l+5}{2l+3}\right)\frac{k_1}{k_2}\left[I_l + \frac{1}{2}\,Q_{l+2}(z)\right] - \frac{1}{2}\,Q_{l+1}(z). \quad (5.6)$$

In the above, Q is the Legendre function of the second kind [13, (8.1.3)] and the argument z is

$$z = (k_1^2 + k_2^2 + \lambda^2)/(2k_1k_2). \quad (5.7)$$

Expression (5.6) is evaluated recursively starting with $l = 0$, in which case I_0 is calculated from the expression [18]

$$I_0 = \frac{3k_1}{2k_2} + \frac{1}{8k_2^2}(3\lambda^2 - 3k_1^2 + k_2^2)\ln\left(\frac{\lambda^2 + (k_1+k_2)^2}{\lambda^2 + (k_1-k_2)^2}\right). \quad (5.8)$$

This integral is computed in three different ways: (i) F_l and F_{l+2} are computed by the IEM, the formula (4.2) is used to approximate the integral on each of the subintervals of partition, and the total integral is obtained by summing-up the integrals obtained for each partition; (ii) same as above with F_l and F_{l+2} obtained through IMSL; and (iii) F_l and F_{l+2} are obtained through the IMSL subroutine at Gauss–Legendre points in each subinterval of partition; the Gauss–Legendre quadrature is used to approximate the integral in each of the subintervals, and the total is obtained by summing-up the results from each partition. The results as a function of the number of subintervals, m, are given in Table II. Here (C-C) stands for Clenshaw–Curtis and (G-L) for Gauss–Legendre. The exact value obtained from (5.6) is 2.66825093E-11. The fact that all three methods converge to a number different from the actual value is due to the truncation error at $T = 50\ fm$.

In the last column of Table II the functions F were obtained from the solution of (5.3) by means of Numerov's method, and the integral was performed using Simpson's rule. The accuracy of one significant figure, achieved with 16×2048 points, did not improve with further increase in the number of integration points. A higher order integration method, the Romberg scheme of order h^{10}, applied on the same Numerov's solution, gave the same low accuracy. The (G-L) + IMSL method gives better results than the (C-C) + IMSL for small values of m. This has already been noted by Sloane [19], and a more detailed comparison between the (G-L) and (C-C) methods can be found in Webb [20]. However, this advantage is offset in applications for which the known functions F are replaced by unknown functions which are the solutions of the Schrödinger equation with a nontrivial potential. In this case the solutions first have to be evaluated by the IEM and, hence, (C-C) + IEM is expected to be the method of choice.

C. *The Case of a Slowly Decaying Potential*

In Subsection A the accuracy of the IEM was discussed for the case $\overline{V}(r) = 0$, i.e., for Riccati–Bessel functions. In

TABLE II

Accuracy of the Integral $I_6(1, 40, 0.7)$ as a Function of m[a]

m	(C-C) + IEM	(C-C) + IMSL	(G-L) + IMSL	Numerov + Simpson
64			−1.72021473E-10	—
128	2.95278631E-11	2.66799012E-11	2.66825063E-11	—
256	2.66829124E-11	2.66825087E-11	2.66825081E-11	—
512	2.66825073E-11	2.66825079E-11	2.66825076E-11	1.65456977E-11
1024	2.66825077E-11	2.66825076E-11	2.66825075E-11	2.01987872E-11
2048	2.66825078E-11	2.66825076E-11	2.66825073E-11	2.19477918E-11

[a] The range of integration is [0, 50] *fm*; the total number of points per partition is 16.

this subsection, the IEM is tested for the case that $\overline{V}(r)$ is a slowly decaying potential of the form $\overline{V}(r) = 1/(r + r^4)$. The r^{-4} decay of this potential occurs in the collision between atoms. We calculate the solution with the IEM for $l = 5$, $k = 5\ fm^{-1}$, and $n = 16$ for various values of the truncation limit T. For each value of T we choose the number of partitions such that $m \simeq kT/\pi$. This is approximately the number of partitions for which highest accuracy was achieved for the evaluation of Riccati–Bessel functions.

Since the analytic solution is not available, the errors were computed by comparing with the IEM results obtained at $T = 900$. Errors in the constant ω, defined in (2.12) are given in column 4 of Table III (for the sake of easier display we represented here the constant ω by a real number β/α).

The asymptotic constant ω, being the most important quantity in the solution, deserves special attention. In this particular real case one obtains from (2.13), by setting $u = 1$ and $v = \omega_T$, the result

$$\omega_T = \frac{-(1/k)\int_0^T F_l \overline{V}(r) R_l\, dr}{1 - (1/k)\int_T^\infty G_l \overline{V}(r) R_l\, dr}.$$

From the above, one finds that the absolute error in ω_T is given by

$$\omega_\infty - \omega_T \approx \varepsilon_1 + \varepsilon_2 \omega_T (1 + \varepsilon_2),$$

where

$$\varepsilon_1 = -\frac{1}{k}\int_T^\infty F_l \overline{V}(r) R_l\, dr \simeq -\varepsilon,$$

$$\varepsilon_2 = -\frac{1}{k}\int_T^\infty G_l \overline{V}(r) R_l\, dr \simeq -\varepsilon,$$

with

$$\varepsilon \simeq \frac{1}{2k}\int_T^\infty \overline{V}(r)\, dr \tag{5.9}$$

and

$$\omega_\infty = -\frac{1}{k}\int_0^\infty F_l \overline{V}(r) R_l\, dr.$$

Hence,

$$|\omega_\infty - \omega_T| \le \varepsilon(1 + \omega_T).$$

Similarly,

$$|\omega_T - \omega_T| \le \bar{\varepsilon}(1 + \omega_T) \tag{5.10a}$$

TABLE III

Error as a Function of T

No. of partitions m	Truncation limit T	ω_T	Numerical error in ω_T	Estimated error (5.10)
166	100	0.3948555996568E-01	3.33E-08	3.3E-08
333	200	0.3948558910348E-01	4.13E-09	4.1E-09
1166	700	0.3948559317246E-01	5.25E-11	5.2E-11
1500	900	0.3948559322496E-01	—	—

TABLE IV

Error in Relation to $\Phi(T)$

Truncation limit $T(fm)$	$\Phi(T)$	Relative error in φ_T
24.752094306051730	8.52E-10	6.7E-12
24.752094304873030	1.18E-12	6.7E-12
24.752094304871433	2.93E-14	7.0E-12
36.543277438730000	1.17E-10	2.4E-11
36.543277437100190	3.25E-12	2.4E-11
36.543277437053801	2.88E-14	2.4E-11

with

$$\bar{\varepsilon} = \frac{1}{2k}\int_T^T \overline{V}(r)\, dr. \tag{5.10b}$$

The estimate of the numerical error in ω_T, based on (5.10) is given in the fifth column of Table III. There is good agreement between the numerical and the estimated values of the error which makes it evident that the $\omega_T's$ are computed accurately and approximate $\omega = \omega_\infty$ within ε given in (5.9). We also attempted to obtain ω_T using Numerov's method. The best approximation, $\omega_T = 0.39485804E - 01$, was obtained for $T = 100$ and with 262,145 points. For increasing T and increasing the number of points the accuracy of Numerov's method deteriorated. It is worthwhile to point out that even for $T = 100$, the IEM already gives higher accuracy than Numerov's method. However, because of the long-range nature of the potential, one has to go to greater length to achieve higher accuracy and, therefore, the IEM clearly becomes the method of choice.

D. *Accuracy of the Solution near a Zero of* $\Phi(T)$

Here we test the effects of choosing the upper truncation limit T near T_0, where $\Phi(T_0) = 0$ and Φ is defined in (2.3b). Again, we choose $V(r) = l(l+1)/r^2$ so that $\Phi(T)$ can be computed by calling IMSL subroutines and the zeros of $\Phi(T)$ are then found by the simple bisection method. Two such zeros are $T_0 = 24.752094304871433$ and $T_0 = 36.543277437053801$. The relative errors in the computed solution for $T \to T_0$ are given in Table IV. This table shows that the choice of T does not affect the accuracy of the numerical solution for the reasons explained in Section II.

VI. SUMMARY

We have described here a method for solving integral equations of the Lippman–Schwinger type which has the following properties: (i) It gives a much higher accuracy than it was ever possible to achieve in finite difference methods. (ii) The computational complexity is linear in the number of points, similar to the situation in finite difference methods. The second property is especially noteworthy because usually matrices associated with the discretization of integral equations are not sparse.

Our method is well suited for applications in which a high accuracy is required. Examples of such applications are: scattering at high energies, calculation of overlap integrals involving highly oscillatory functions, and atomic collisions in the presence of slowly decaying potentials.

We plan to expand the method, which is applied here to the case of positive energies, also, to negative energies, as well as to nonlocal potentials.

ACKNOWLEDGMENTS

The participation of Lan Xu in the early stages of this work is noted, and also, useful comments from several physics colleagues, such as Dr. H. Lee at Argonne National Laboratory, Professor C. Chandler at the University of New Mexico, and Dr. J. Friar at Los Alamos National Laboratory, are gratefully acknowledged.

REFERENCES

1. E. A. Coddington and I. N. Levinson, *Theory of ODE* (McGraw–Hill, New York, 1955).
2. R. H. Landau, *Quantum Mechanics II. A Second Course in Quantum Theory* (Wiley-Interscience, New York, 1989).
3. L. I. Schiff, *Quantum Mechanics,* 3rd ed. (McGraw–Hill, New York, 1968).
4. R. W. Hamming, *Numerical Methods for Scientists and Engineers,* McGraw-Hill, New York, 1962.
5. C. W. Clenshaw and A. R. Curtis, *Numer. Math.* **2,** 197 (1960).
6. L. Greengard, *SIAM J. Numer. Anal.* **28**(4), 1071 (1991).
7. L. Greengard and V. Rokhlin, *Commun. Pure Appl. Math.* **44,** 419 (1991).
8. D. Gottlieb and S. Orszag, *Numerical Analysis of Spectral Methods* (SIAM, Philadelphia, 1977).
9. E. Buendia, R. Guardiola, and M. Montoya, *J. Comput. Phys.* **68,** 188 (1987).
10. A. D. Raptis and J. R. Cash, *Comput. Phys. Commun.* **36,** 113 (1985).
11. G. Avdelas and T. E. Simos, *Comput. Math. Appl.* **31**(2), 85 (1996).
12. G. H. Golub and C. H. Van Loan, *Matrix Computations* (Johns Hopkins Univ. Press, Baltimore, 1983.
13. M. Abramovitz and I. Stegun, (Eds.), *Handbook of Mathematical Functions* (Dover, New York, 1972).
14. C. Van Loan, *Computational Framework for Fast Fourier Transform,* SIAM, Philadelphia, 1992.
15. L. M. Delves and J. L. Mohamed, *Computational Methods for Integral Equations,* Cambridge University Press, Cambridge, 1985.
16. J. Stoer and R. Bulirsch, *Introduction to Numerical Analysis,* 2nd ed., Springer-Verlag, New York, 1993.
17. J. L. Friar, *J. Comput. Phys.* **28** (1978), 426.
18. M. I. Haftel and F. Tabakin, *Nucl. Phys. A* **158,** 1 (1970).
19. I. Sloane, *J. Math. Phys.* **21,** 1032 (1980).
20. D. Webb, unpublished.